Chapter 5

Reconstruction in a Liquid Argon TPC

Should the title of this chapter reflect more of the original work which is discussed within? e.g. Shower Reconstrucion in a Liquid Argon TPC? Although it is a general reconstruction chapter, everything in Shower Reconstruction in LArTPCs is original.

The use of LArTPCs in future high-precision projects, such as long-baseline neutrino experiments, is very well motivated by the unprecedented spatial and energy resolution available to detectors utilising the techonology. In order to take advantage of all this accessible information, accurate reconstruction must be developed to perform pattern recognition and energy determination for use by the proceeding analyses. The techniques and status of reconstruction in LArTPCs is the subject of this chapter, with particular focus on novel methods developed for the reconstruction of electromagnetic showers.

The implementation of the reconstruction algorithms discussed in this chapter utilises the Liquid Argon Software framework (LArSoft), developed at FNAL and shared between all experiments in the LAr program. LArSoft will be overviewed in Section 5.1 before the structural and calorimetric reconstructions are discussed in Sections 5.2 and 5.2.3 respectively. The development of new techniques in the reconstruction of showers will compose the main discussion in this chapter and is contained in Section 5.3.

5.1 The LArSoft Framework

The Liquid Argon Software (LArSoft) [144–147] collaboration supports the development, use, sharing and distributing of code utlitised by all LAr experiments at FNAL. The LArSoft framework is written in C++ and built on *art* [136, 137], the event-processing system develop at FNAL and used by offline code developed for most experiments hosted at the lab. As data from most LArTPC experiments share a similar basic format, LArSoft is envisioned to be agnostic to the detector specifics and provide a common interface, infrastructure and

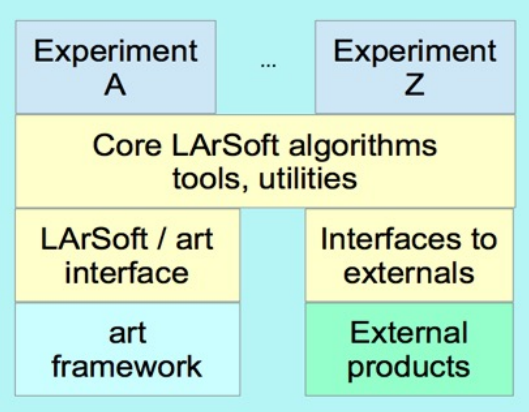

Fig. 5.1 The LArSoft architecture, highlighting support for both common and experiment-specific algorithms and methods and the interfacing with other packages. Taken from [146].

algorithms for simulation, reconstruction and analysis. Along with vastly reducing duplicated effort, this also allows access to the most advanced software developments for smaller collaborations who otherwise may not have the required resources.

LArSoft provides well defined interfaces to various external packages, such as GENIE [148] and GEANT4 [149], and access by particular experiments utilises configurable descriptions of the detector geometry, the electronics, detector response and other unique features. This structure is demonstrated in Figure 5.1. This architecture ensures a flexible structure which facilitates the addition and evolution of algorithms and with contigency for future developments to be introduced with ease.

The *art* framework provides an interface to the information stored for each event by user-written 'modules' and handles execution by processing each entry and making the data available to these plug-in modules. Additionally, 'services', which exist outside of the event structure, are provided and may be used to obtain general information such as detector geometry or LAr properties whenever needed. The two main module types, named `Analyzers` (sic) and `Producers`, can access the data products stored in a particular event and, in the case of `Producers`, have the ability to place data into the event for use in future processes. All modules, regardless of their type, have only `const` access to the existing information in the event. Configuration of an *art* job utilises the custom Fermilab Hierarchical Configuration Language (*fhicl*, pronounced 'fickle') which may be used to define the modules (including their order) and services to be run and to provide run-time parameters for use by these products.

The end-to-end configuration for a given experiment involves the following standard stages: generation (provided by a generator, such as GENIE), propagation (executed with GEANT4), detector response simulation, and reconstruction. The results from the first three

steps aim to reproduce as closely as possible the expectations from real data, with the same reconstruction applied to both the simulated output from the detector and data. The processes are configured, using `Producer` modules, in *art* using *fhicl*, generally separated into four jobs representing each of the stages.

LArSoft was initially developed for use in ArgoNeuT in around 2011 and has since progressed into the large collaboration which it is today, with more than 100 code authors spanning multiple experiments. The constant progression of algorithms have resulted in very well-developed, advanced simulation and reconstruction tools with corresponding shared expertise. The recent uses of LArSoft reconstruction on real data, in MicroBooNE [150] and the 35 ton (Chapter **??**), are providing an excellent test of the efficacy of the simulation along with the validation of reconstruction applied to data. The current reconstruction chain is discussed in Section 5.2 and the process of calorimetry in a LArTPC and the LArSoft implementation is the subject of Section 5.2.3.

Until recently, convincing electromagnetic shower reconstruction has not existed within LArSoft. Despite this being a major advantage of LArTPCs, it is particularly challenging and requires significant investment of resources to fully understand. This motivated the development of new algorithms within the LArSoft framework, BlurredCluster and EMShower, which will be discussed in detail in Section 5.3.

5.2 The Reconstruction Chain

Reconstruction in LArSoft is the process of forming particle objects, with enough information to be able to perform identification, from the raw charge read out by the anode planes. The process may be considered as three main components: calibrating the raw charge to remove detector effects; pattern recognition; calorimetry. The general workflow is shown schematically in Figure 5.2.

5.2.1 From Charge to Hits

The charge induced and collected on the readout wires is modified by detector effects which must be well understood in order to be properly accounted for. The measured waveform, $p(t)$, obtained from the signal $s(t)$, measured as a function of time t, can be represented in pseudocode as

$$p(t) = (s(t) \otimes e(t) \otimes f(t)) + n(t), \tag{5.1}$$

where e is the electronics response, f is the field response and n is the noise in the detector. Together, $e(t) \otimes f(t)$ are referred to as the detector response.

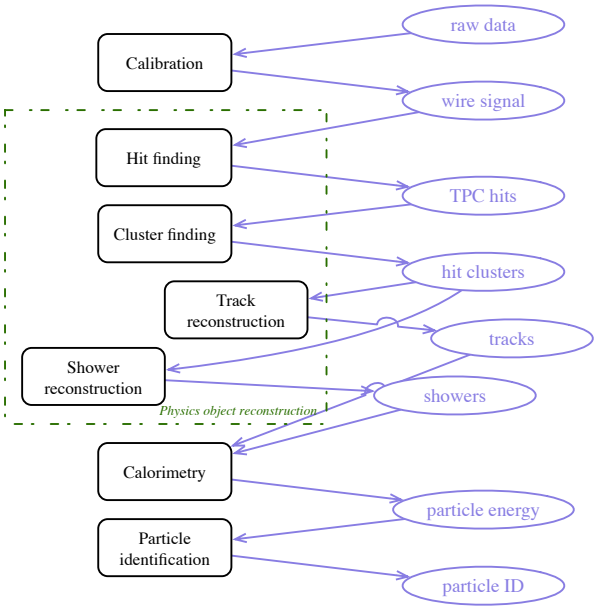

Fig. 5.2 The LArSoft reconstruction workflow to produce 3D reconstructed objects from the raw charge read out by the anode wires [146]. The status of the reconstruction is shown on the right, with the various algorithms and their outputs represented on the left.

The first step in the reconstruction, referred to as the 'deconvolution stage', involves removing these detector responses. This proceeds by subtracting the noise profile from the measured waveform before Fourier transforming into frequency space and dividing out the field and electronics components. The detector responses must be accurate and the models used have been developed at test stands to ensure they best represent the detector effects. This process is applied in reverse during the detector simulation stage of the simulation to reproduce the expectations from the data as much as possible.

Following the deconvolution stage, the waveforms all have the form of a unipolar pulse. The reconstruction proceeds with 'hit finding', with the purpose to accurately determine the properties of the collected charge. In particular, the peak time, width and total charge of the 'hit's are pertinent for future reconstruction algorithms. This is typically achieved by fitting a Gaussian to the pulse and using this to aid the determination of the hit properties. The result of the deconvolution and hit finding stages are represented for simulated hits on three separate planes in Figure 5.3.

Due to the wrapped wires, multiple hits will be reconstructed on each channel, one for each possible wire segment. The final stage of hit processing is to perform disambiguation to select the correct hit for use in subsequent algorithms. As previously discussed (Section 3.3.2.1 and Section 4.3.1.1), this is trivial in the far detector design as the wire wrapping angles are chosen such that no induction wire segment crosses each collection channel more

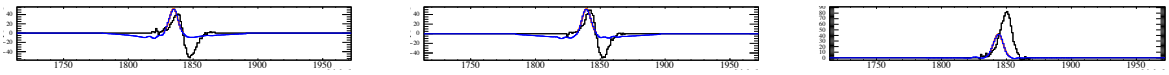

(a) U plane. (b) V plane. (c) Z plane.

Fig. 5.3 The process of deconvolution and hit finding to determine the correct charge from the measured pulses on the readout wires. Each 2D plane is represented as charge (ADC) as a function of time (tick). In each case, the black waveform represents the raw measurement, the blue shows the outcome of deconvolution and the pink peak indicates the reconstructed hit. Note the normalisation of the deconvoluted signal has been fixed to provide a factor four amplification for illustratory purposes. The shift in time and shape is a result of the deconvolution from the electronics response (demonstrated in Figure **??**).

than once. In the 35 ton, the slight difference in angle between the two induction planes results in 'triple points', where there are hits on each plane almost instantaously, which facilitates a deduction of the correct induction channel hits.

5.2.2 Object Reconstruction

The next typical stage of the reconstruction following hit finding is the process of forming 2D objects, or 'clustering'. In LArSoft, all 2D objects, regardless of their topology, are named 'clusters' and are simply a collection of hits identified as being associated with a common ionising particle. These 2D structures exist only on a given plane and do not have contributions from multiple views; the extension to 3D reconstruction involves combining numerous clusters between the views. Multiple cluster algorithms exist in LArSoft, each designed for different specialisations.

An example 2D view of a ν_μCC event, simulated in a reduced far detector volume, is shown in Figure 5.4. This particular interaction is a deep inelastic scattering producing, along with the muon, multiple final state protons and a very high energy π^+ meson. The outcome of hit reconstruction is demonstrated in Figure 5.4a and the result of applying clustering to these hits is displayed in Figure 5.4b, with each colour representing a separate cluster.

Combining 2D information from multiple views in a LArTPC enables the formation of 3D objects. In LArSoft, several 3D products exist: 'space points', 'vertices', 'tracks' and 'showers'. Space points are a form of 3D hit, defined simply by a point in the detector Cartesian geometry, and vertices are a specific example of these locations created to represent an important part of the event (e.g. the neutrino interation point or even just a track start). Tracks and showers are more complete objects which represent individual particles and contain associated properties relevant to the topology of each. Tracking is relatively advanced in LArSoft, with multiple track fitters shown to produce well-formed track objects efficiently; shower reconstruction is less so and will be discussed in detail in Section 5.3.

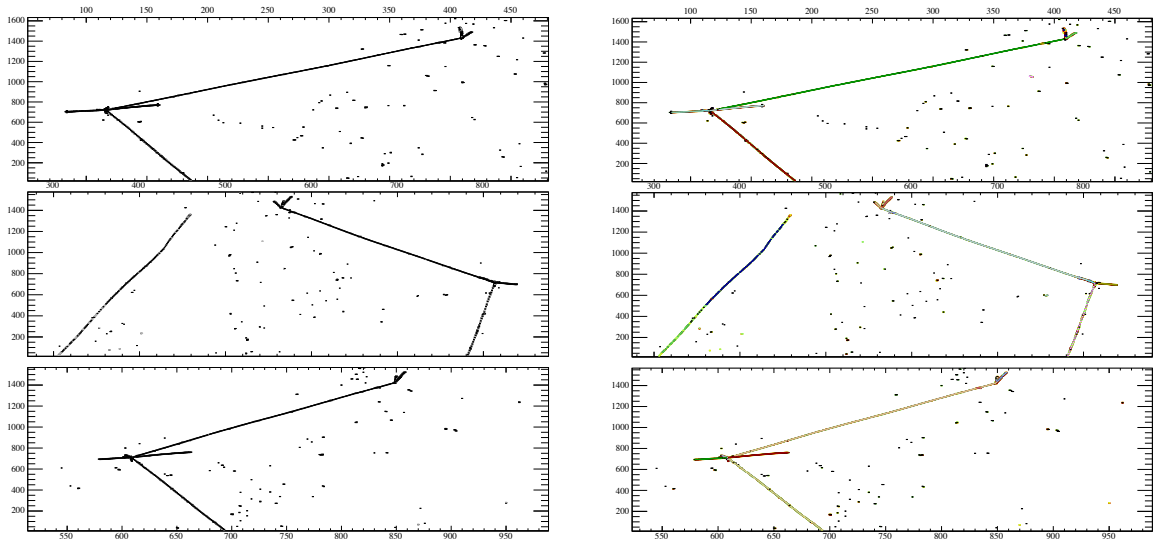

(a) Hit reconstruction.

(b) Cluster reconstruction.

Fig. 5.4 Demonstration of 2D reconstruction in LArSoft on a simulated ν_μCC event. The result of hit finding is shown in Figure 5.4a, where each black rectangle represents a separate hits, and the grouping of these hits into clusters is illustrated in Figure 5.4b, where blocks of hits sharing a common colour are associated to the same cluster object.

The result of applying track reconstruction to the ν_μCC interaction discussed in Figure 5.4 is shown in Figure 5.5. As with clusters, each colour represents a unique track object and it is clear from Figure 5.5a that hits across multiple planes contribute to a given track. A complementary view is also shown in Figure 5.5b, where the objects are represented in two orthogonal views in the detector coordinate system.

It is worth noting the approach to forming the eventual 3D objects, from which particle identification and analysis may be executed, is not unique. The method outlined above is most relevent to the shower reconstruction discussed in Section 5.3 and is the most common chain used in most LArSoft processing; however, progress is being made on an additional technique which focusses directly on 3D reconstruction. This is called ‘Wire-Cell’ [151] and utilises a tomographic method, following the LArTPC principal that each plane observes the same amount of ionisation electrons, to build up a 3D image of the event. This may then be characterised to find the properties of the particles and make the track and shower products. All reconstruction methods utilise the same information provided by the detector but not necessarily in the same order.

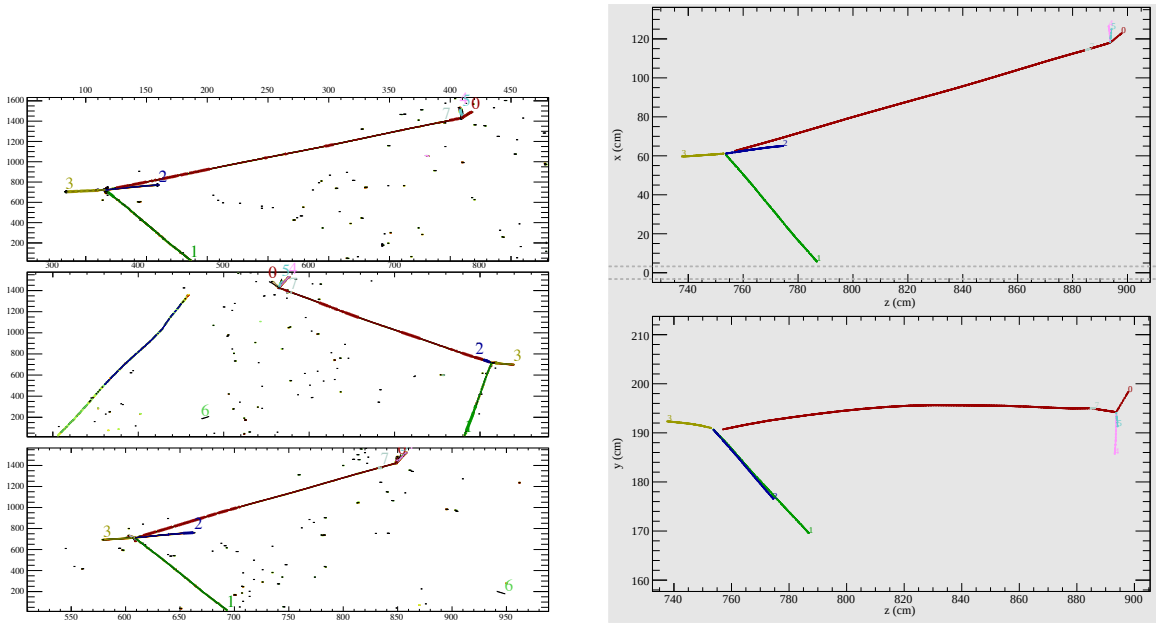

(a) 2D view; wire vs tick for multiple wire planes.

(b) 3D view; x-z and y-z othogonal planes.

Fig. 5.5 Demonstration of 3D reconstruction in LArSoft on a simulated ν_μCC event. Each colour represents a unique 3D track object, with information shared between each of the anode planes; this is evident in Figure 5.5a. An additional view is demonstrated in Figure 5.5b where two orthogonal planes of the detector geometry are shown.

5.2.3 Calorimetry

The possibility of extremely precise energy measurements is a hugely attractive feature of LArTPCs and is achieved by careful calibration of the charge recieved from the drift electrons. There are two distinct calibrations which must be conducted to ensure reliable calorimetric measurements; setting the ADC to energy translation and determining the shower energy conversion from the total deposited charge. These will be discussed in Sections 5.2.3.1 and 5.2.3.2 respectively.

5.2.3.1 Energy Determination

Following deconvolution and hit finding, the charge carried by each packet of electrons is understood as the Gaussian integral of the hit and has units 10 e^- (often just 'ADC' in certain following plots). This is converted to an energy

5.2.3.2 Shower Energy Reconstruction

5.3 Shower Reconstruction in LArTPCs

5.3.1 Showers Overview

5.3.2 BlurredCluster Algorithm

5.3.3 EMShower Algorithm

5.3.4 Track/Shower Separation

5.3.5 Performance of the Reconstruction

References

[1] Sheldon L Glashow. Partial-symmetries of weak interactions. *Nuclear Physics*, 22(4):579–588, 1961.

[2] Steven Weinberg. A Model of Leptons. *Phys. Rev. Lett.*, 19(21):1264–1266, 1967.

[3] G. Aad, et al. Observation of a new particle in the search for the Standard Model Higgs boson with the ATLAS detector at the LHC. *Physics Letters B*, 716(1):1–29, 2012.

[4] S. Chatrchyan, et al. Observation of a new boson at a mass of 125 GeV with the CMS experiment at the LHC. *Physics Letters, Section B: Nuclear, Elementary Particle and High-Energy Physics*, 716(1):30–61, 2012.

[5] Tara Shears. The Standard Model. *Phil. Trans. Roy. Soc. Lond.*, A370:805–817, 2012.

[6] S M Bilenky. Neutrino in standard model and beyond. *Physics of Particles and Nuclei*, 46(4):475–496, 2015.

[7] John Ellis. Outstanding questions: Physics beyond the Standard Model. *Phil. Trans. Roy. Soc. Lond.*, A370:818–830, 2012.

[8] Y Fukuda, et al. Evidence for Oscillation of Atmospheric Neutrinos. *Phys. Rev. Lett.*, 81(8):1562–1567, 1998.

[9] Q R Ahmad, et al. Direct Evidence for Neutrino Flavor Transformation from Neutral-Current Interactions in the Sudbury Neutrino Observatory. *Phys. Rev. Lett.*, 89(1):11301, 2002.

[10] Wolfgang Pauli. Open letter to the participants of the conference in Tubingen, 1930.

[11] E Fermi. Trends to a Theory of beta Radiation. (In Italian). *Nuovo Cim.*, 11:1–19, 1934.

[12] E Fermi. Versuch einer Theorie der β-Strahlen. I. *Zeitschrift für Physik*, 88(3):161–177, 1934.

[13] F. Wilson. Fermi's Theory of Beta Decay. *American Journal of Physics*, 36(12):1150–1160, 1968.

[14] G M Lewis. *Neutrinos*. Wykeham publications, London; Winchester, 1970.

[15] C M G Lattes, et al. Processes Involving Charged Mesons. *Nature*, 159:694–697, 1947.

[16] C M G Lattes, G P S Occhialini, and C F Powell. Observations on the Tracks of Slow Mesons in Photographic Emulsions. 1. *Nature*, 160:453–456,486–492, 1947.

[17] R Brown, et al. Observations With Electron Sensitive Plates Exposed to Cosmic Radiation. *Nature*, 163:82, 1949.

[18] C L Cowan, et al. Large Liquid Scintillation Detectors. *Phys. Rev.*, 90(3):493–494, 1953.

[19] F. Reines and C. L. Cowan. A proposed experiment to detect the free neutrino, 1953.

[20] F. Reines and C. L. Cowan. Detection of the free neutrino. *Physical Review*, 92(3):830–831, 1953.

[21] C L Cowan, et al. Detection of the Free Neutrino: a Confirmation. *Science*, 124(3212):103–104, 1956.

[22] Raymond Davis Jr. and Don S Harmer. Attempt to observe the $Cl^{37}(\bar{\nu}e^{-})Ar^{37}$ reaction induced by reactor antineutrinos. *Bull. Am. Phys. Soc.*, 4:217, 1959.

[23] G Danby, et al. Observation of High-Energy Neutrino Reactions and the Existence of Two Kinds of Neutrinos. *Phys. Rev. Lett.*, 9(1):36–44, 1962.

[24] M. L. Perl, et al. Evidence for anomalous lepton production in e^{+}-e^{-} annihilation. *Physical Review Letters*, 35(22):1489–1492, 1975.

[25] G J Feldman, et al. Inclusive Anomalous Muon Production in $e^{+}e^{-}$ Annihilation. *Phys. Rev. Lett.*, 38(3):117–120, 1977.

[26] J Burmester, et al. Anomalous muon production in $e^{+}e^{-}$ annihilations as evidence for heavy leptons. *Physics Letters B*, 68(3):297–300, 1977.

[27] D. DeCamp, et al. Determination of the number of light neutrino species. *Physics Letters B*, 231(4):519–529, 1989.

[28] B Adeva, et al. A determination of the properties of the neutral intermediate vector boson Z0. *Physics Letters B*, 231(4):509–518, 1989.

[29] M Z Akrawy, et al. Measurement of the Z0 mass and width with the opal detector at LEP. *Physics Letters B*, 231(4):530–538, 1989.

[30] P Aarnio, et al. Measurement of the mass and width of the Z0-particle from multi-hadronic final states produced in $e^{+}e^{-}$ annihilations. *Physics Letters B*, 231(4):539–547, 1989.

[31] S. Schael, et al. Precision electroweak measurements on the Z resonance. *Physics Reports*, 427(5-6):257–454, 2006.

[32] K. Kodama, et al. Observation of tau neutrino interactions. *Physics Letters, Section B: Nuclear, Elementary Particle and High-Energy Physics*, 504(3):218–224, 2001.

[33] H A Bethe. Energy Production in Stars. *Phys. Rev.*, 55(5):434–456, 1939.

[34] John N Bahcall, Neta A Bahcall, and Giora Shaviv. Present Status of the Theoretical Predictions for the ^{37}Cl Solar-Neutrino Experiment. *Phys. Rev. Lett.*, 20(21):1209–1212, 1968.

[35] John N. Bahcall, Aldo M. Serenelli, and Sarbani Basu. New Solar Opacities, Abundances, Helioseismology, and Neutrino Fluxes. *The Astrophysical Journal*, 621(1):L85–L88, 2005.

[36] B. T. Cleveland, et al. Update on the measurement of the solar neutrino flux with the Homestake chlorine detector. *Nuclear Physics B (Proceedings Supplements)*, 38(1-3):47–53, 1995.

[37] John N Bahcall, M H Pinsonneault, and G J Wasserburg. Solar models with helium and heavy-element diffusion. *Rev. Mod. Phys.*, 67(4):781–808, 1995.

[38] J. N. Abdurashitov, et al. Results from SAGE (The Russian-American gallium solar neutrino experiment). *Physics Letters B*, 328(1-2):234–248, 1994.

[39] P. Anselmann, et al. Solar neutrinos observed by GALLEX at Gran Sasso. *Physics Letters B*, 285(4):376–389, 1992.

[40] W. Hampel, et al. GALLEX solar neutrino observations: Results for GALLEX IV. *Physics Letters, Section B: Nuclear, Elementary Particle and High-Energy Physics*, 447:127–133, 1999.

[41] E. Gaisser, T. K.; Engel, R.; Resconi. *Cosmic Rays and Particle Physics*. Cambridge University Press, 1990.

[42] T J Haines, et al. Calculation of Atmospheric Neutrino-Induced Backgrounds in a Nucleon-Decay Search. *Phys. Rev. Lett.*, 57(16):1986–1989, 1986.

[43] K S Hirata, et al. Experimental study of the atmospheric neutrino flux. *Physics Letters B*, 205(2):416–420, 1988.

[44] W Anthony Mann. Atmospheric neutrinos and the oscillations bonanza. *Int. J. Mod. Phys.*, A15S1:229–256, 2000.

[45] B Pontecorvo. Neutrino Experiments and the Problem of Conservation of Leptonic Charge. *Sov. Phys. JETP*, 26:984–988, 1968.

[46] V Gribov and B Pontecorvo. Neutrino astronomy and lepton charge. *Physics Letters B*, 28(7):493–496, 1969.

[47] B Pontecorvo. Mesonium and anti-mesonium. *Sov. Phys. JETP*, 6:429, 1957.

[48] D Casper, et al. Measurement of atmospheric neutrino composition with the IMB-3 detector. *Phys. Rev. Lett.*, 66(20):2561–2564, 1991.

[49] R Becker-Szendy, et al. Electron- and muon-neutrino content of the atmospheric flux. *Phys. Rev. D*, 46(9):3720–3724, 1992.

[50] Y Fukuda, et al. Atmospheric vμve ratio in the multi-GeV energy range. *Physics Letters B*, 335(2):237–245, 1994.

[51] J N Bahcall. Solar Models and Solar Neutrinos. *Physica Scripta*, 2005(T121):46, 2005.

[52] Ziro Maki, Masami Nakagawa, and Shoichi Sakata. Remarks on the Unified Model of Elementary Particles. *Progress of Theoretical Physics*, 28(5):870, 1962.

[53] John N Bahcall, Concepción M Gonzalez-Garcia, and Carlos Pena-Garay. Before and After: How has the SNO NC measurement changed things? *Journal of High Energy Physics*, 2002(07):54, 2002.

[54] A Yu. Smirnov. The MSW effect and solar neutrinos. In *Neutrino telescopes. Proceedings, 10th International Workshop, Venice, Italy, March 11-14, 2003. Vol. 1+2*, pages 23–43, 2003.

[55] L Wolfenstein. Neutrino oscillations in matter. *Phys. Rev. D*, 17(9):2369–2374, 1978.

[56] S P Mikheev and A Yu. Smirnov. Resonance Amplification of Oscillations in Matter and Spectroscopy of Solar Neutrinos. *Sov. J. Nucl. Phys.*, 42:913–917, 1985.

[57] S P Mikheev and A Yu. Smirnov. Resonant amplification of neutrino oscillations in matter and solar neutrino spectroscopy. *Nuovo Cim.*, C9:17–26, 1986.

[58] K Eguchi, et al. First Results from KamLAND: Evidence for Reactor Antineutrino Disappearance. *Phys. Rev. Lett.*, 90(2):21802, 2003.

[59] T Araki, et al. Measurement of Neutrino Oscillation with KamLAND: Evidence of Spectral Distortion. *Phys. Rev. Lett.*, 94(8):81801, 2005.

[60] Abhijit Bandyopadhyay, et al. The Solar neutrino problem after the first results from KamLAND. *Phys. Lett.*, B559:121–130, 2003.

[61] Pedro Cunha de Holanda and A Yu. Smirnov. LMA MSW solution of the solar neutrino problem and first KamLAND results. *JCAP*, 0302:1, 2003.

[62] G L Fogli, et al. Evidence for Mikheyev-Smirnov-Wolfenstein effects in solar neutrino flavor transitions. *Phys. Lett.*, B583:149–156, 2004.

[63] Thomas Mannel. Theory and Phenomenology of CP Violation. *Nuclear Physics B - Proceedings Supplements*, 167:115–119, 2007.

[64] Tommy Ohlsson, He Zhang, and Shun Zhou. Radiative corrections to the leptonic Dirac *CP*-violating phase. *Phys. Rev. D*, 87(1):13012, 2013.

[65] Tommy Ohlsson, He Zhang, and Shun Zhou. Probing the leptonic Dirac CP-violating phase in neutrino oscillation experiments. *Physical Review D - Particles, Fields, Gravitation and Cosmology*, 87(5):1–8, 2013.

[66] DUNE Collaboration. Long-Baseline Neutrino Facility (LBNF) and Deep Underground Neutrino Experiment (DUNE): The LBNF and DUNE Projects. 1, 2016.

[67] K Abe, et al. Physics potential of a long-baseline neutrino oscillation experiment using a J-PARC neutrino beam and Hyper-Kamiokande. *Progress of Theoretical and Experimental Physics*, 2015(5):053C02, 2015.

[68] F Kaether, et al. Reanalysis of the Gallex solar neutrino flux and source experiments. *Physics Letters B*, 685(1):47–54, 2010.

[69] J N Abdurashitov, et al. Measurement of the solar neutrino capture rate with gallium metal. III. Results for the 2002–2007 data-taking period. *Phys. Rev. C*, 80(1):15807, 2009.

[70] B Aharmim, et al. Combined analysis of all three phases of solar neutrino data from the Sudbury Neutrino Observatory. *Phys. Rev. C*, 88(2):25501, 2013.

[71] A Gando, et al. Reactor on-off antineutrino measurement with KamLAND. *Phys. Rev. D*, 88(3):33001, 2013.

[72] R Wendell, et al. Atmospheric neutrino oscillation analysis with subleading effects in Super-Kamiokande I, II, and III. *Phys. Rev. D*, 81(9):92004, 2010.

[73] M G Aartsen, et al. Determining neutrino oscillation parameters from atmospheric muon neutrino disappearance with three years of IceCube DeepCore data. *Phys. Rev. D*, 91(7):72004, 2015.

[74] P Adamson, et al. Measurement of Neutrino and Antineutrino Oscillations Using Beam and Atmospheric Data in MINOS. *Phys. Rev. Lett.*, 110(25):251801, 2013.

[75] P Adamson, et al. Electron Neutrino and Antineutrino Appearance in the Full MINOS Data Sample. *Phys. Rev. Lett.*, 110(17):171801, 2013.

[76] K Abe, et al. Precise Measurement of the Neutrino Mixing Parameter θ_{23} from Muon Neutrino Disappearance in an Off-Axis Beam. *Phys. Rev. Lett.*, 112(18):181801, 2014.

[77] P Adamson, et al. First measurement of muon-neutrino disappearance in NOvA. *Phys. Rev. D*, 93(5):51104, 2016.

[78] M C Gonzalez-Garcia, Michele Maltoni, and Thomas Schwetz. Updated fit to three neutrino mixing: status of leptonic CP violation. *Journal of High Energy Physics*, 2014(11):52, 2014.

[79] Ivan Esteban, et al. Updated fit to three neutrino mixing: exploring the accelerator-reactor complementarity. *Journal of High Energy Physics*, 2017(1):87, 2017.

[80] F P An, et al. Observation of Electron-Antineutrino Disappearance at Daya Bay. *Phys. Rev. Lett.*, 108(17):171803, 2012.

[81] J K Ahn, et al. Observation of Reactor Electron Antineutrinos Disappearance in the RENO Experiment. *Phys. Rev. Lett.*, 108(19):191802, 2012.

[82] K Abe, et al. Observation of Electron Neutrino Appearance in a Muon Neutrino Beam. *Phys. Rev. Lett.*, 112(6):61802, 2014.

[83] P Adamson, et al. First Measurement of Electron Neutrino Appearance in NOvA. *Phys. Rev. Lett.*, 116(15):151806, 2016.

[84] K Abe, et al. Combined Analysis of Neutrino and Antineutrino Oscillations at T2K. *Phys. Rev. Lett.*, 118(15):151801, 2017.

[85] V N Aseev, et al. Upper limit on the electron antineutrino mass from the Troitsk experiment. *Phys. Rev. D*, 84(11):112003, 2011.

[86] Ch Kraus, et al. Final results from phase II of the Mainz neutrino mass search in tritium β-decay. *The European Physical Journal C - Particles and Fields*, 40(4):447–468, 2005.

[87] Planck Collaboration, et al. Planck 2013 results. XVI. Cosmological parameters. *Astronomy & Astrophysics*, 571:A16, 2014.

[88] DUNE Collaboration. Long-Baseline Neutrino Facility (LBNF) and Deep Underground Neutrino Experiment (DUNE): The Physics Program for DUNE at LBNF. 2, 2015.

[89] DUNE Collaboration. Long-Baseline Neutrino Facility (LBNF) and Deep Underground Neutrino Experiment (DUNE): Long Baseline Neutrino Facility for DUNE. 3, 2016.

[90] DUNE Collaboration. Long-Baseline Neutrino Facility (LBNF) and Deep Underground Neutrino Experiment (DUNE): The DUNE Detectors at LBNF. 4, 2016.

[91] S. Amerio, et al. Design, construction and tests of the ICARUS T600 detector. *Nuclear Instruments and Methods in Physics Research, Section A: Accelerators, Spectrometers, Detectors and Associated Equipment*, 527(3):329–410, 2004.

[92] C Anderson, et al. The ArgoNeuT detector in the NuMI low-energy beam line at Fermilab. *Journal of Instrumentation*, 7(10):P10019, 2012.

[93] F Cavanna, et al. LArIAT: Liquid Argon In A Testbeam. 2014.

[94] R Acciarri, et al. Design and construction of the MicroBooNE detector. *Journal of Instrumentation*, 12(02):P02017, 2017.

[95] B Baller, et al. Liquid Argon Time Projection Chamber research and development in the United States. *Journal of Instrumentation*, 9(05):T05005, 2014.

[96] David R Nygren. The Time Projection Chamber - A New 4pi Detector for Charged Particles. *eConf*, C740805(PEP-0144):58–78, 1974.

[97] Carlo Rubbia. The Liquid Argon Time Projection Chamber: A New Concept For Neutrino Detectors.pdf, 1977.

[98] Mitch Soderberg. The MicroBooNE Proposal, 2008.

[99] V Chepel and H Araújo. Liquid noble gas detectors for low energy particle physics. *Journal of Instrumentation*, 8(04):R04001, 2013.

[100] P. Derwent, et al. Proton Improvement Plan-II (PIP-II). Technical Report December, 2013.

[101] Patrick Huber and Joachim Kopp. Two experiments for the price of one? The role of the second oscillation maximum in long baseline neutrino experiments. *Journal of High Energy Physics*, 2011(3):13, 2011.

[102] LBNE Collaboration. Long-Baseline Neutrino Experiment (LBNE) Project: The LBNE Project. 1, 2012.

[103] LBNE Collaboration. Long-Baseline Neutrino Experiment (LBNE) Project: Detectors At The Near Site. 3, 2012.

[104] LBNE Collaboration. Long-Baseline Neutrino Experiment (LBNE) Project: Liquid Argon Detector At The Far Site. 4, 2012.

[105] Margherita Buizza Avanzini. The LAGUNA-LBNO Project. *Physics Procedia*, 61:524–533, 2015.

[106] HEPAP Subcommittee. Building for Discovery: Strategic Plan for U.S. Particle Physics in the Global Context. 2014.

[107] M. Convery and Z. Djurcic. The 35-Ton Liquid Argon TPC Prototype for the Long Baseline Neutrino Experiment (Poster). In *Neutrino 2014 Conference Proceedings*, 2014.

[108] T Kutter. Proposal for a Full-Scale Prototype Single-Phase Liquid Argon Time Projection Chamber and Detector Beam Test at CERN. Technical Report CERN-SPSC-2015-020. SPSC-P-351, CERN, Geneva, 2015.

[109] I De Bonis and Others. LBNO-DEMO: Large-scale neutrino detector demonstrators for phased performance assessment in view of a long-baseline oscillation experiment. 2014.

[110] CERN Courier. Neutrinos take centre stage.

[111] D Finley, et al. Work at FNAL to achieve long electron drift lifetime in liquid argon. 2006.

[112] R Andrews, et al. A system to test the effects of materials on the electron drift lifetime in liquid argon and observations on the effect of water. *Nucl. Instrum. Meth.*, A608:251–258, 2009.

[113] A Curioni, et al. A regenerable filter for liquid argon purification. *Nuclear Instruments and Methods in Physics Research Section A: Accelerators, Spectrometers, Detectors and Associated Equipment*, 605(3):306–311, 2009.

[114] B Rebel, et al. Results from the Fermilab materials test stand and status of the liquid argon purity demonstrator. *J. Phys. Conf. Ser.*, 308:12023, 2011.

[115] P Cennini, et al. Argon purification in the liquid phase. *Nuclear Instruments and Methods in Physics Research Section A: Accelerators, Spectrometers, Detectors and Associated Equipment*, 333(2):567–570, 1993.

[116] P Benetti, et al. A three-ton liquid argon time projection chamber. *Nuclear Instruments and Methods in Physics Research Section A: Accelerators, Spectrometers, Detectors and Associated Equipment*, 332(3):395–412, 1993.

[117] F Arneodo, et al. Performance of a liquid argon time projection chamber exposed to the CERN West Area Neutrino Facility neutrino beam. *Phys. Rev. D*, 74(11):112001, 2006.

[118] G Carugno, et al. Electron lifetime detector for liquid argon. *Nuclear Instruments and Methods in Physics Research Section A: Accelerators, Spectrometers, Detectors and Associated Equipment*, 292(3):580–584, 1990.

[119] Alan Hahn, et al. The LBNE 35 Ton Prototype Cryostat. In *Proceedings, 21st Symposium on Room-Temperature Semiconductor X-ray and Gamma-ray Detectors (RTSD 2014): Seattle, WA, USA, November 8-15, 2014*, page 7431158, 2014.

[120] Terry Tope and Others. Extreme argon purity in a large, non-evacuated cryostat. *AIP Conf. Proc.*, 1573:1169–1175, 2014.

[121] M Adamowski, et al. The Liquid Argon Purity Demonstrator. *Journal of Instrumentation*, 9(07):P07005, 2014.

[122] C Bromberg, et al. Design and operation of LongBo: a 2 m long drift liquid argon TPC. *Journal of Instrumentation*, 10(07):P07015, 2015.

[123] David Montanari and Others. First scientific application of the membrane cryostat technology. *AIP Conf. Proc.*, 1573:1664–1671, 2014.

[124] David Montanari, et al. Performance and results of the LBNE 35 ton membrane cryostat prototype. *Physics Procedia*, 67:308–313, 2015.

[125] Fermi National Accelerator Laboratory Visual Media Services, 2015.

[126] T Alion. 35∼ton Geometry, 2014.

[127] 35ton. 35 ton Photon Detectors. *NOT PUBLISHED YET*.

[128] A Artikov, et al. Design and construction of new central and forward muon counters for {CDF} {II}. *Nuclear Instruments and Methods in Physics Research Section A: Accelerators, Spectrometers, Detectors and Associated Equipment*, 538(1–3):358–371, 2005.

[129] M. Stancari. 35 ton Counter Locations, 2015.

[130] G De Geronimo, et al. Front-End ASIC for a Liquid Argon TPC. *IEEE Transactions on Nuclear Science*, 58(3):1376–1385, 2011.

[131] C Thorn, et al. Cold Electronics Development for the LBNE LAr TPC. *Physics Procedia*, 37:1295–1302, 2012.

[132] R Herbst, et al. Design of the SLAC RCE Platform: A general purpose ATCA based data acquisition system. In *2014 IEEE Nuclear Science Symposium and Medical Imaging Conference (NSS/MIC)*, pages 1–4, 2014.

[133] J.T. Anderson, et al. SiPM Signal Processor User Manual. Technical report, 2016.

[134] N. Barros, et al. The Penn Trigger Board. Technical report, 2016.

[135] K Biery, et al. artdaq: An Event-Building, Filtering, and Processing Framework. *IEEE Transactions on Nuclear Science*, 60(5):3764–3771, 2013.

[136] art website.

[137] C Green, et al. The art framework. *Journal of Physics: Conference Series*, 396(2):22020, 2012.

[138] J. Freeman. Courtesy of John Freeman, Fermilab, 2014.

[139] D S Akerib and Others. LUX-ZEPLIN (LZ) Conceptual Design Report. 2015.

[140] A Blatter, et al. Experimental study of electric breakdowns in liquid argon at centimeter scale. *Journal of Instrumentation*, 9(04):P04006, 2014.

[141] N McConkey, et al. Cryogenic CMOS cameras for high voltage monitoring in liquid argon. *Journal of Instrumentation*, 12(03):P03014, 2017.

[142] 35∼ton Phase∼II LAr filling monitored by camera system, 2016.

[143] L Bagby, et al. 35∼ton Noise. *DUNE Document Database*, 1834, 2016.

[144] LArSoft website.

[145] Eric D Church. LArSoft: A Software Package for Liquid Argon Time Projection Drift Chambers. 2013.

[146] Ruth Pordes and Erica Snider. The Liquid Argon Software Toolkit (LArSoft): Goals, Status and Plan. *Proceedings of Science*, ICHEP2016:182, 2016.

[147] E L Snider. LArSoft: Toolkit for Simulation, Reconstruction and Analysis of Liquid Argon TPC Neutrino Detectors. In *22nd International Conference on Computing in High Energy and Nuclear Physics (CHEP 2016) San Francisco, CA, October 14-16, 2016*.

[148] C Andreopoulos, et al. The {GENIE} neutrino Monte Carlo generator. *Nuclear Instruments and Methods in Physics Research Section A: Accelerators, Spectrometers, Detectors and Associated Equipment*, 614(1):87–104, 2010.

[149] J Allison, et al. Geant4 developments and applications. *IEEE Transactions on Nuclear Science*, 53(1):270–278, 2006.

[150] R Acciarri and Others. Michel Electron Reconstruction Using Cosmic-Ray Data from the MicroBooNE LArTPC. *Submitted to: JINST*, 2017.

[151] BNL. Wire-Cell LArTPC Reconstruction. Technical report.